SANS investigation of self-assembling dendrimers in organic solvents

Pappannan Thiyagarajan,[a]* Fanwen Zeng,[b] C. Y. Ku[a] and Steven C. Zimmerman[b]*

[a]*IPNS, Argonne National Laboratory, Argonne, IL60439, USA*

[b]*Department of Chemistry, University of Illinois, Urbana, IL61801, USA*

The self-assembly behaviour of tetraacids **1a**–**c** and tetraester **4** in $CDCl_3$ and [$^2H_8$]tetrahydrofuran {[$^2H_8$]THF} has been investigated by the small-angle neutron scattering (SANS) technique. The experimental SANS data were compared with simulated scattering data derived from structural models proposed previously for the aggregates. These studies suggest that dendritic monomers **1b**,**c** self-assemble into cyclic hexameric aggregates, whereas **1a** forms a large tubular aggregate in $CDCl_3$. Further study on **1c** in $CDCl_3$ as a function of concentration suggests that the cyclic hexameric aggregates strongly interact with each other at higher concentrations. The control compound **4** was shown to be monomeric in both solvents.

There is significant current interest in organic compounds that form stable, discrete aggregates in solution.[1] These aggregates may have a particular function or they may serve as synthetic intermediates for the construction of larger, covalently linked nano- or meso-structures. In this regard, hydrogen-bond mediated self-assembly is a powerful approach because the directionality of hydrogen bonding allows control over the aggregate structure, while its strength in apolar solvents provides a considerable enthalpic driving force to overcome the disfavourable entropy of aggregation. One successful approach to forming discrete aggregates is to target closed assemblies, such as those formed in cyclic arrays of monomers. An added benefit of the cyclic aggregation approach is the cooperativity which often manifests itself in highly stable and discrete self-assembled structures.

One of the continuing unsolved challenges in this area is to characterize the aggregate structure in solution. Because there is no single method for unambiguously determining the number density and structure of aggregates present, the characterization is often based on a combination of several indirect methods.[2] The commonly used techniques are size-exclusion chromatography (SEC), ^{1}H NMR spectroscopy, vapour pressure osmometry (VPO), UV–VIS and IR spectroscopy, and sometimes mass spectrometry. We recently reported that dendritic tetraacids **1b**,**c** self-assemble into cyclic hexamer **2**, whereas **1a** forms a series of linear aggregates such as **3** (Fig. 1).[3] Hexamer **2**, whose structure was supported by SEC, VPO, and comparison with a covalently linked model, is the largest known discrete abiotic aggregate formed by weak interactions.[4] Herein, we report the use of small-angle neutron scattering (SANS) technique to characterize the self-assembly behaviour of **1a**–**c** and test the previously proposed models.

SANS and small-angle X-ray scattering (SAXS) are direct techniques which can yield unique information about the structure and interactions of macromolecules with sizes in the range of 10 to 1000 Å. A distinguishing feature of neutron scattering compared to X-ray scattering is that neutrons interact with atomic nuclei, while X-rays interact with the electron clouds of the atoms. This property renders neutron scattering very sensitive to different isotopes, such as proton and deuterium whose coherent lengths are quite different.[5] SANS is one of the highly applied neutron scattering techniques for the characterization of macromolecules and several reviews dealing with the application of this technique for biological systems have been published.[6] This technique allows extraction of form factors, which are descriptions of macromolecular size and shape, and particle–particle structure factors in solutions. SANS has also been demonstrated to provide structural information on supramolecular assemblies in their native state in aqueous solution[7] and their interparticle interactions.[8b]

Materials and Methods

Materials

The synthesis and characterization of compounds **1a**–**c** and **4** were described previously[3] and material was available from the prior studies. [$^2H_1$]Chloroform and [$^2H_8$]tetrahydrofuran, purchased from Cambridge Isotope Laboratory, were used directly.

SANS measurements

SANS experiments of compounds **1a**–**c** and **4** were performed in $CDCl_3$. The self-assembly behaviour of compounds **1c** and **4** was also investigated in [$^2H_8$]THF to study the effect of this solvent, which is more competitive toward hydrogen-bonding interactions. The corresponding solution was injected into a Suprasil cylindrical cell with a 2 mm pathlength (volume = 0.7 ml). SANS data were collected at the Intense Pulsed Neutron Source of Argonne National Laboratory, using the time-of-flight SANS instrument, Small Angle Neutron Diffractometer (SAND).[9a] This instrument uses pulsed neutrons derived from spallation with wavelengths in the range 0.5–14 Å and a fixed sample-to-detector distance of 2 m. The scattered neutrons are measured using a 128×128 array of position sensitive, gas filled, 40×40 cm^2, proportional counters with the wavelengths measured by time-of-flight through binning the pulse to 68 constant $Dt/t = 0.05$ time channels. The size range in a SANS experiment depends on the range of momentum transfer Q [see eqn. (2)] which is determined by the geometry of the instrument and the range of wavelengths of the neutrons. Given the characteristics of the SAND at the Intense Pulsed Neutron Source (IPNS), useful SANS data in the Q range 0.0035–0.8 Å^{-1} can be obtained in a single measurement. The data for each sample is corrected for the backgrounds from the instrument, the Suprasil cell, and the solvent as well as for detector non-linearity.[9b] Data are presented on absolute scale by using the known scattering cross-section of a silica gel sample.

Small-angle neutron scattering

The differential scattering cross-section $I(Q)$ measured as a function of momentum transfer Q by SANS is a convolution

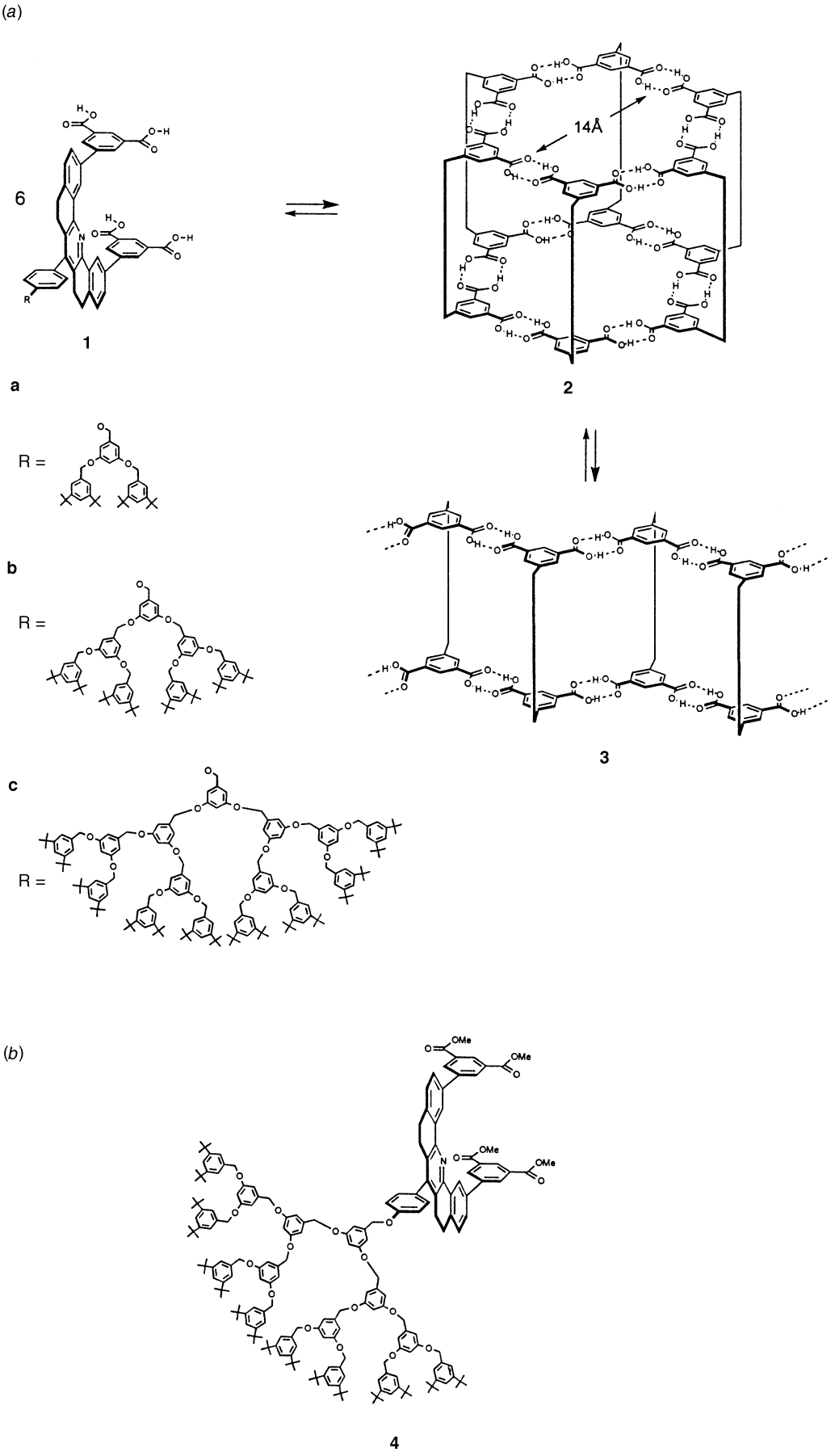

Fig. 1 (*a*) Dendritic tetraacids **1a**–**c** and the proposed cyclic hexameric aggregate **2** and linear aggregate **3**, (*b*) tetraester **4**

of two terms, namely, intraparticle correlations $P(Q)$ and interparticle correlations $S(Q)$.

$$I(Q)=nP(Q)S(Q) \quad (1)$$

In eqn. (1), n is the number of particles per unit volume and

$$Q=4\pi\lambda^{-1}\sin\theta \quad (2)$$

where λ is the wavelength of neutrons and 2θ is the scattering angle.

The intraparticle structure factor $P(Q)$ is defined as

$$P(Q)=\left\{\sum_{i,j} b_i b_j \exp[iQ(r_i-r_j)]\right\} \quad (3)$$

and the interparticle structure factor

$$S(Q)=\frac{1}{N}\left\{\sum_{i=1}^{N}\sum_{j=1}^{N} \exp[iQ(R_i-R_j)]\right\} \quad (4)$$

In eqn. (3), r_i and r_j are the position vectors of the atoms in a particle and b_i and b_j are the scattering lengths[5] of atoms i and j and the braces indicate that averaging for all orientations of the particles is taken. In general, the scattering power of an atom depends on the isotope.[5] Eqn. (3) can be used to calculate the scattering from the particle, if atomic coordinates are available. In eqn. (4), R_i and R_j are the position vectors of the particle centres and N is the total number of particles.

In the case of dilute solutions the particles are far apart and $S(Q)$ in the low Q region will oscillate around unity and hence $I(Q)$ is predominantly due to $P(Q)$. The $I(Q)$ data can be readily analysed to obtain the correct size, shape and molecular mass of the particle. At higher concentrations where the excluded volume effects become significant the size and molecular mass parameters derived from the low-Q region become lower in values. This is due to the increased effect of $S(Q)$ on $I(Q)$ and one has to decompose $I(Q)$ to obtain the $P(Q)$ and $S(Q)$ terms prior to analysis. This step, however, requires information on the size and morphology of the particles as well as the interaction potentials. Under these conditions it is possible to obtain the surface potentials of the colloidal objects.[8]

Analysis of SANS data

At the low-Q region, the experimental scattering intensity $I(Q)$ *vs.* Q data can be used to obtain size information by using eqn. (5)[11] which is an approximation of eqn. (1) in the low-Q region.

$$I(Q)=I(0)\exp(-Q^2R_g^2/3) \quad (5)$$

where

$$I(0)=n(\rho_p-\rho_s)^2\,V^2 \quad (6)$$

In eqn. (6), ρ_p and ρ_s are the scattering length densities ($\rho=\Sigma b_i/V$) of the particles and the solvents, V is the volume of the particle, and b_i is the scattering length of individual atoms. The radius of gyration, R_g is the root-mean-squared distances of all of the atoms to the centroid of the scattering volume of the particle. This parameter is shape independent and one needs to know the shape of the particle in order to derive sizes in terms of the familiar physical dimensions. For example, for a sphere with a radius of R, $R_g^2=0.6R^2$ and for an ellipsoid, $R_g^2=(a^2+d^2+c^2)/5$ where a, d, c are the semiaxes of an ellipsoid. The value of R_g is obtained from the absolute value of the slope (k) of a line in the natural log of $I(Q)$ *vs.* Q^2 plot (Guinier plot)[11] in the Q region where $QR_g \# 1.0$, as $R_g^2=3k$. In dilute solutions where the interparticle interactions are either nonexistent or minimal, this value will represent the true size of the particle. However, in the presence of interparticle interactions the value of R_g will be smaller and this value has to be denoted as apparent value. In the absence of any other concentration dependent effects, such as aggregation, it is possible to obtain the true R_g of the particle by the linear extrapolation of measured R_g values at several concentrations. The magnitude of the slope of the curve (second virial coefficient) in the apparent R_g *vs.* concentration plot yields qualitative information on the interparticle interactions.

In the case of polydisperse systems, the R_g and $I(0)$ values are respectively the Z-averaged and mass-averaged quantities. For example, the Z-averaged R_g value is defined as

$$\langle R_g^2\rangle=\frac{\sum N_i M_i^2 (R_g^2)_i}{\sum N_i M_i^2} \quad (7)$$

where N_i and M_i and $(R_g)_i$ are the number density, molecular mass, and radius of gyration of the aggregates of type i, respectively.

The shape of the scattering particles can be analysed by fitting the scattering pattern in the whole Q range by either using the analytical functions for the form factors of different geometrical objects,[11] or by calculating the scattering pattern using a suitable molecular model, as was done for proteins using eqn. (3).[10] The molecular models of compounds **1a**–**c** and **4** and their possible aggregate structures were constructed with the Macromodel program[12] on a Silicon Graphics workstation. Because of the limitations on the number of atoms used, the dendrimer substituents and the tetraacid core unit were minimized separately and then covalently linked. Each structure was first minimized using molecular mechanics: MM2 force field with the Polak–Ribier conjugate gradient method of optimization. These minimized structures were then further minimized by molecular dynamics with automatic set-up parameters of 300 K, initial temperature, 10 ps run with a 15 fs timestep using SHAKE and zero momentum.

The atomic coordinates of the structures derived from the modelling studies were used to calculate the scattering patterns. It is important to state that we used only the atomic coordinates of the molecular models for calculating the scattering curves, but did not use the neutron scattering cross-sections of individual atoms. What this means is that the shape of the scattering curve for a given system is appropriate, but the scaling is not. We arbitrarily scaled the calculated scattering data and compared the shapes with the experimental data to test the validity of the proposed models. In the case of 10.6 mM $CDCl_3$ solution of **1a** none of the aggregate models generated by the Macromodel program could explain the measured scattering data (discussed later) and hence modelling using the form factor for a hollow cylinder was used. The form factor of a cylindrical shape particle with or without a hollow inner portion (tube *vs.* rod) can be written as

$$A(\boldsymbol{Q})=\frac{2\sin(Q_aL/2)}{Q_aL/2}\left[\frac{J_1(Q_cR_o)}{Q_cR_o}-\frac{R_i}{R_o}\left(\frac{R_i}{R_o}\right)^2\frac{J_1(Q_cR_i)}{Q_cR_i}\right] \quad (8)$$

where L is the length of the cylinder, R_o is the outer radius of the cylinder, R_i is the inner radius of the cylinder, Q_a is the component of $\boldsymbol{Q}$ in the axial direction, Q_c is the component of $\boldsymbol{Q}$ in the cross-section plane, and J_1 is the first-order Bessel function of the first kind. The orientationally averaged particle structure factor used to fit is

$$P(Q)=\frac{V^2}{4\pi}\int_{-1}^{1} d\mu \int_{0}^{2\pi} d\omega |A(\boldsymbol{Q})|^2 \quad (9)$$

where $V=\pi R_o^2 L$.

Results and Discussion

Fig. 2 shows the measured SANS data for **1c** in $CDCl_3$ at three concentrations. Each curve is superimposed by the calculated SANS data from the coordinates generated for the cyclic hexamer **2** (see Fig. 1) proposed for this system. It is

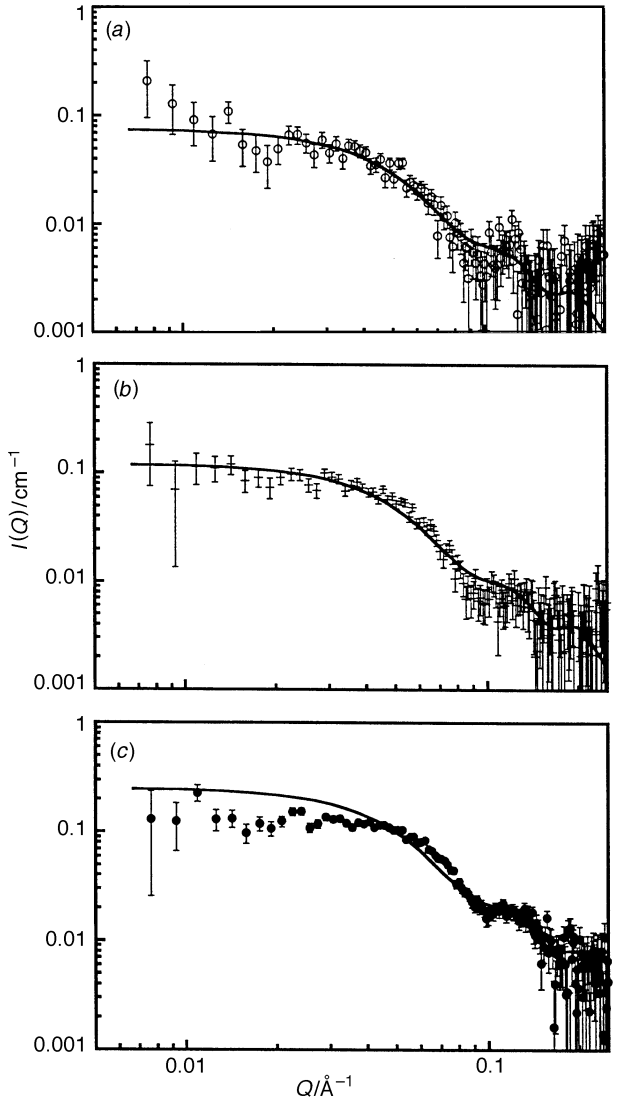

Fig. 2 Experimental SANS data for **1c** in $CDCl_3$ at three concentrations: (*a*) 12 mg ml^{-1}, (*b*) 24 mg ml^{-1} and (*c*) 50 mg ml^{-1}. The calculated scattering pattern (—) from the coordinates generated for the cyclic hexamer model proposed for this system is superimposed on the experimental data.

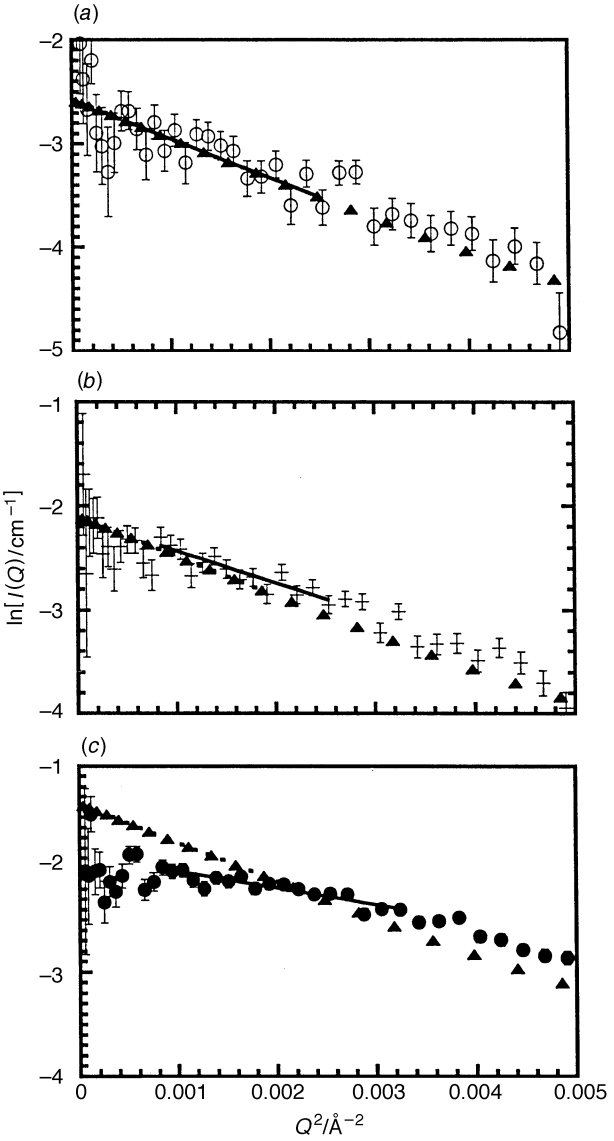

Fig. 3 Corresponding Guinier plots for the data in Fig. 2. The Guinier plots for the calculated curves (+) are shown in each case. The value of the slopes in the experimental data (—) decreases with increasing concentration; all of them are smaller than that for the calculated data.

clearly demonstrated that the calculated and measured data agree reasonably well for a solution with a concentration of 3.8 mM (12 mg ml^{-1}) [Fig. 2(*a*)] and the agreement becomes poorer with increasing concentration. The actual disagreement is in the low-Q region of the high concentration sample which suggests the presence of interparticle interactions between these hexamer aggregates in $CDCl_3$. The interparticle effects can be seen better in the corresponding Guinier plots (Fig. 3) which exhibit decreasing slopes (decrease of apparent R_g values) with increasing concentration, when compared to the calculated data for the cyclic hexamer. The calculated SANS data for the cyclic hexamer yields an R_g of 33.6 Å, while the apparent R_g values for the measured samples with a monomer concentration of 3.8 mM (12 mg ml^{-1}), 7.6 mM (24 mg ml^{-1}) and 15.7 mM (50 mg ml^{-1}) are 30.4, 28.9 and 23.7 Å, respectively. Fig. 4 shows the linear dependence of apparent R_g as a function of concentration. The R_g value at infinite dilution from Fig. 4 is 33.1 Å which agrees quite well with the expected value of 33.6 Å on the basis of the proposed model. Thus the cyclic hexamer model (see Fig. 1) proposed for **1c** in $CDCl_3$ is consistent with the SANS results. However, it is noteworthy to mention that SANS also suggests the presence of concentration-dependent interactions between these aggregates at the high concentration range investigated here.

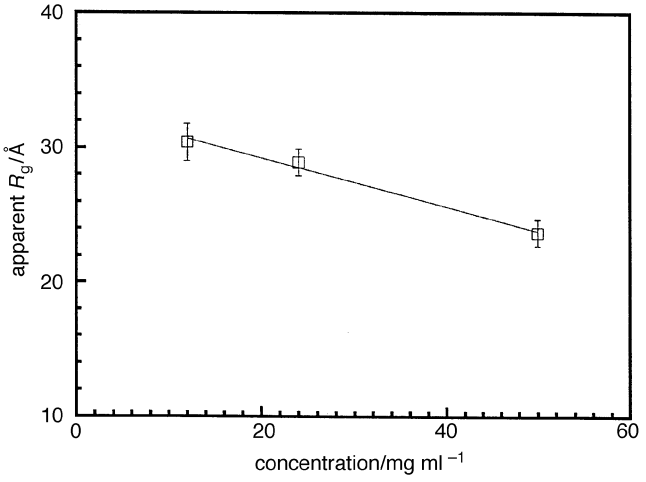

Fig. 4 Apparent R_g values as a function of concentration for **1c** in $CDCl_3$. The linearity implies that the particles are intact but interact strongly. The extrapolated R_g value at infinite dilution agrees well with the R_g value calculated for the cyclic hexamer.

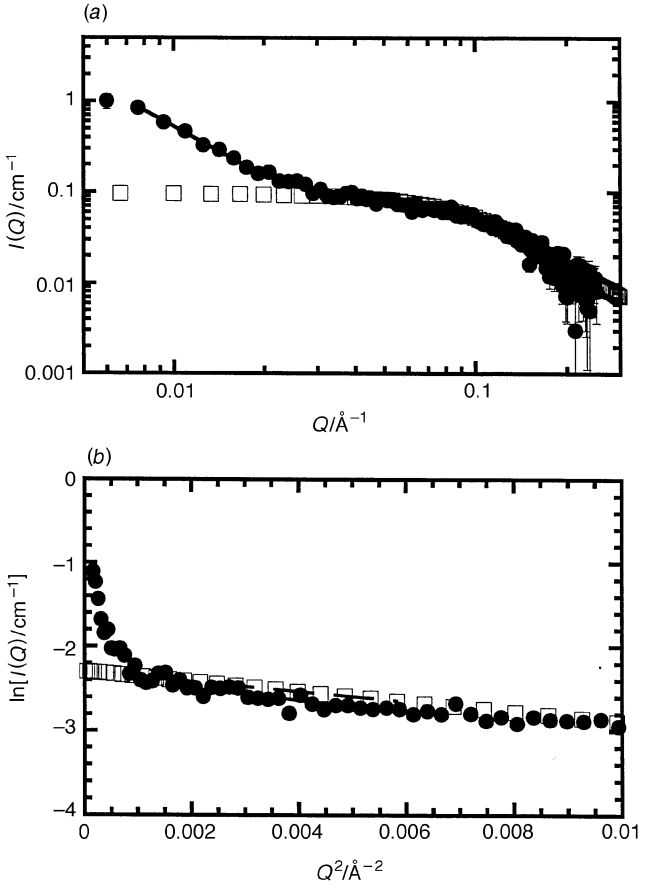

Fig. 5 (*a*) Experimental SANS data of a 6.3 mM solution of **1c** in [$^2H_8$]THF (\$) along with the calculated data for a monomer (%). (*b*) Guinier plots for the data in (*a*).

When **1c** is dissolved in [$^2H_8$]THF the aggregation properties change. The $I(Q)$ data and the corresponding Guinier curves for a solution of **1c** in [$^2H_8$]THF at a concentration of 8.2 mM are shown in Fig. 5. Compound **1c** was proposed to exist as a monomer in this media as THF competes with the hydrogen-bonding contacts thus preventing aggregate formation. The measured $I(Q)$ data for this is compared with the calculated SANS data for a monomer. The R_g value of 13.5 Å for the calculated SANS curve agrees reasonably well with the experimental R_g value of 14.6 ± 1 Å obtained from the middle-Q region of the data. Also the data in the high-Q region for both the experimental and the calculated data for a monomer agree quite well. However, in the low-Q region, the two data sets do not agree. Interestingly, the low-Q region of the experimental data exhibits a power law [$I(Q) \# Q^{-1.8}$] which points to extremely large structures resembling mass fractals.[13] Nevertheless this unusual SANS curvature in the low-Q region is not reproducible. For example, in a different run, the experimental SANS data fit to the calculated value for a dimeric structure. The differences between runs may originate from a slow disassembly process of the hexameric aggregate.[14]

To demonstrate the appropriateness of the SANS technique for examining this class of macromolecules, as well as to probe the effect of solvent on conformation, tetraester **4** was investigated in both $CDCl_3$ and [$^2H_8$]THF. Tetraester **4**, a close analogue of **1c**, was shown previously to exist as a monomer in both solvents due to the absence of hydrogen-bonding sites.[3] The SANS data collected for **4** in $CDCl_3$ and [$^2H_8$]THF at a concentration of 8.0 mM are shown in Fig. 6. These results validate the monomer model proposed for this system (see Fig. 1). Thus, these data show that the experimental scattering patterns are identical to the calculated ones for the monomer. The large difference in the scaling of data for **4** in $CDCl_3$ and

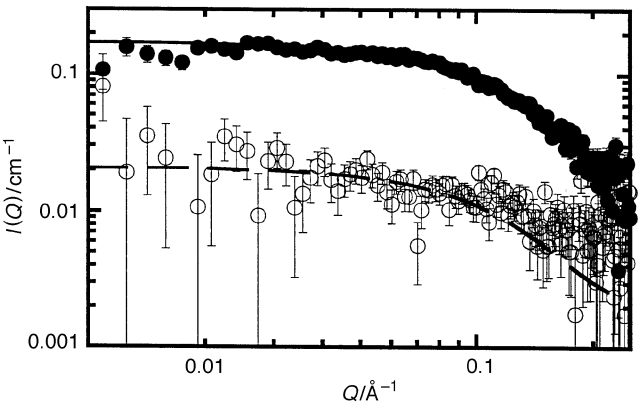

Fig. 6 Experimental SANS data for 16 mg ml^{-1} **4** in [$^2H_8$]THF (\$) and in $CDCl_3$ (#). The lines are the calculated scattering patterns for the monomer. The different scaling between these data sets is due to the difference in contrast provided by the solvent for the scattering from the monomer.

[$^2H_8$]THF is due to different contrasts [see eqn. (6)] provided by the different scattering length densities of the solvents $CDCl_3$ (3.16×10^{10} cm^{-2}) and [$^2H_8$]THF (6.36×10^{10} cm^{-2}). It is evident that the contrast for neutron scattering from these particles is higher in [$^2H_8$]THF when compared to that in $CDCl_3$ as seen from the low signal intensity and large error bars for the latter, even though both samples used similar beam times.

Tetraacids **1** with second- and first-generation dendritic substituents were also investigated. Experimental SANS data for an 8.5 mM solution of **1b** in $CDCl_3$ along with the calculated data derived from a cyclic hexameric aggregate are shown in Fig. 7. The experimental R_g of 27.1 ± 1 Å agrees quite well with that from the calculated data ($R_g = 28.6$ Å). The shapes of the scattering patterns also agree well in the whole Q region thus validating the correctness of the proposed model for this system.

Previous SEC dilution study in methylene chloride showed that the aggregation of tetraacid **1a** is concentration dependent. This behaviour, as well as the broadness of the SEC peak, suggested that **1a** forms a series of linear aggregates. Molecular modelling studies suggested that this preference resulted from the small size of the first-generation dendritic substituent which could be accommodated in the linear aggregate structure (Fig. 1). Non-specific aggregation was also observed in the SANS studies which suggest the formation of large and polydisperse aggregates in a 10.6 mM $CDCl_3$ solution of **1a** (Fig. 8). This Fig. shows the measured SANS data and calculated form factors for linear aggregates with 8 and 20 monomers. The Guinier plot for the measured data has at least two different

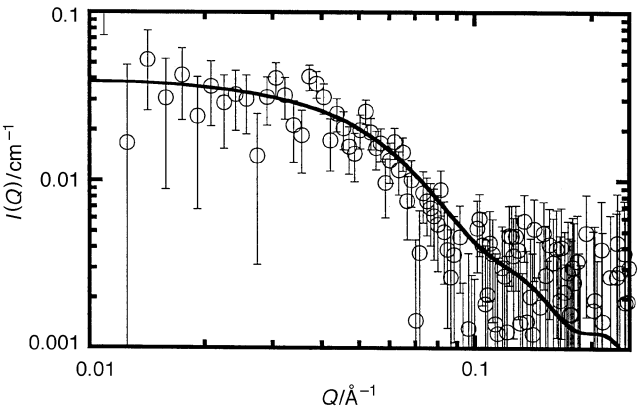

Fig. 7 SANS data for **1b** in $CDCl_3$ (#) along with the calculated data for a cyclic hexamer. The data agree quite well, validating the proposed model.

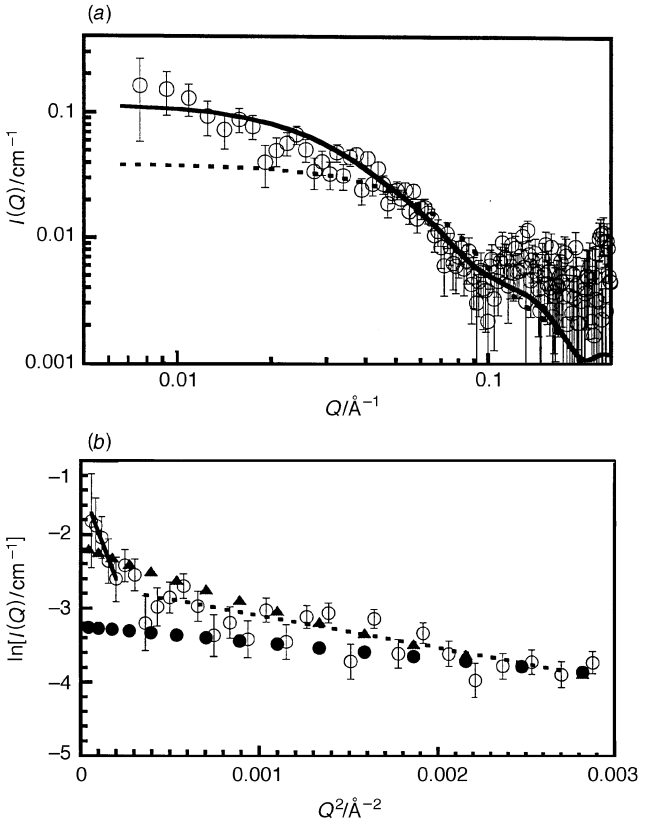

Fig. 8 (*a*) SANS data for **1a** in $CDCl_3$ (#) along with the calculated scattering patterns for a linear aggregate with 8 monomers (,) and with 20 monomers (—). The scattering pattern has a secondary peak which indicates a more ordered structure. The linear aggregate model does not explain the data well. (*b*) Guinier plots for the data in (*a*). Experimental data (#), $R_g = 137 \pm 35$ Å (—), $R_g = 36 \pm 5$ Å (,); calculated data for linear aggregates with 8 monomers ($) and with 20 monomers (+). The experimental data indicate the presence of polydispersity as at least two different linear regions are seen.

linear regions corresponding to R_g values of 36 ± 5 and 137 ± 35 Å. On the other hand, the R_g values for the calculated data for the linear aggregates of 8 and 20 monomers, respectively, are 24.6 and 50.6 Å. The scattering patterns for linear aggregates with different polymer indices were calculated, but none of them could fit the secondary peak at $Q = 0.12$ Å^{-1} in the experimental data. The best fit of the scattering data was however accomplished by using eqn. (9) for a hollow cylindrical aggregate with an outer radius of 31 Å, inner radius of 26–28 Å and a length of 49 Å. It is not obvious how **1a** can form such a structure, except perhaps an open helical assembly formed from an extremely flat and extended monomer. Further SANS and molecular modelling studies are needed to elucidate the exact aggregate structure for compound **1a**.

Conclusions

Hydrogen-bond mediated self-assembling dendrimers have been studied by a variety of techniques and structural models have been proposed based on the results of SEC, NMR and VPO studies. Small-angle neutron scattering (SANS) was shown to be a direct and powerful technique for studying these systems in different solvents. Scattering data were calculated from the atomic coordinates generated from the proposed models and compared with the measured scattering data. This offers a direct way to compare the validity of the models and thus increase our understanding of these systems.

The SANS studies provide strong support for the cyclic hexamer model previously proposed for **1b**,**c** in $CDCl_3$. SANS further suggests a concentration dependent interaction between these hexameric aggregates. The ester analogue **4** was studied in both THF and $CDCl_3$ and found to exist as a monomer, as expected. Compound **1a** seems to form large and non-discrete aggregates. However, the previously proposed linear aggregate model could not explain the experimental data rather the aggregate may have a thin, hollow, cylindrical structure.

This work was supported by the US Department of Energy, Office of Basic Energy Sciences, Division of Material Sciences, under Contract W-31-109-Eng-38 to IPNS. S.C.Z. gratefully acknowledges support from the National Institutes of Health (GM39782). F. Z. thanks the University of Illinois Department of Chemistry for a fellowship. We gratefully acknowledge the technical support provided by D. G. Wozniak at IPNS.

References

1 (*a*) J-M. Lehn, *Angew. Chem., Int. Ed. Engl.*, 1990, **29**, 1304; (*b*) J. S. Lindsey, *New J. Chem.*, 1991, **15**, 153; (*c*) D. S. Lawrence, T. Jiang and M. Levett, *Chem. Rev.*, 1995, **95**, 2229; (*d*) J. F. Stoddart and D. Philp, *Angew Chem., Int. Ed. Engl.*, 1996, **35**, 1154.
2 (*a*) J. P. Mathias, E. E. Simanek and G. M. Whitesides, *J. Am. Chem. Soc.*, 1994, **116**, 4326; (*b*) G. M. Whitesides, E. E. Simanek, J. P. Mathias, C. T. Seto, D. N. Chin, M. Mammen and D. M. Gordon, *Acc. Chem. Res.*, 1995, **28**, 37; (*c*) N. Branda, R. Wyler and J. Rebek Jr., *Science*, 1994, **263**, 1267; (*d*) M. R. Ghadiri, J. R. Granja, R. A. Milligan, D. E. McRee and N. Khazanovich, *Nature* (*London*), 1993, **366**, 324; (*e*) E. E. Schrier, *J. Chem. Educ.*, 1968, **45**, 176.
3 S. C. Zimmerman, F. Zeng, D. E. C. Reichert and S. V. Kolotuchin, *Science*, 1996, **271**, 1095.
4 S. C. Zimmerman, *Curr. Opin. Colloid Interfac. Sci.*, in press.
5 G. E. Bacon, *Neutron Diffraction*, Oxford University Press, Melbourne, 3rd edn., 1975.
6 (*a*) B. Jacrot, *Rep. Prog. Phys.*, 1976, **39**, 911; (*b*) H. B. Stuhrmann and A. Miller, *J. Appl. Crystallogr.*, 1978, **11**, 325; (*c*) L. A. Feigin and D. I. Svergun, *Structure Analysis by Small Angle X-Ray and Neutron Scattering*, Plenum, New York, 1987.
7 (*a*) B. Jacrot, *Comp. Virol.*, 1981, **17**, 129; (*b*) P. Thiyagarajan and D. M. Tiede, *J. Phys. Chem.*, 1994, **98**, 10 343; (*c*) R. P. Hjelm Jr., P. Thiyagarajan and H. A. Alkan, *J. Phys. Chem.*, 1992, **96**, 8653.
8 (*a*) S. H. Chen, *Annu. Rev. Phys. Chem.*, 1986, **37**, 351; (*b*) D. S. Jayasuriya, N. Tcheurekdjian, C. F. Wu, S. H. Chen and P. Thiyagarajan, *J. Appl. Crystallogr.*, 1988, **21**, 843.
9 (*a*) R. K. Crawford, P. Thiyagarajan, J. E. Epperson, F. Trouw, R. Kleb, D. Wozniak and D. Leach, *Proc. 13th International Collaboration on Advanced Neutron Sources*, Switzerland, Oct 11–14, 1995, *PSI-Proc*, 1996, **95–02**, 99–117; (*b*) P. Thiyagarajan, J. E. Epperson, R. K. Crawford, J. M. Carpenter, T. E. Klippert and D. G. Wozniak, *J. Appl. Crystallogr.*, 1997, **30**, in press.
10 P. Thiyagarajan, S. J. Henderson and A. Joachimiak, *Structure*, 1996, **4**, 79.
11 A. Guinier and G. Fournet, *Small Angle Scattering of X-Rays*, John Wiley & Sons, New York, 1955.
12 W. C. Still, Macromodel 3.5a, Columbia University, New York, 1992.
13 (*a*) J. Feder, *Fractals*, Plenum, New York, 1988; (*b*) T. Freltoft, J. K. Kjems and S. K. Sinha, *Phys. Rev. B*, 1986, **33**, 269; (*c*) P. McMahon and I. Snook, *J. Chem. Phys.*, 1996, **105**, 2223.
14 F. Zeng and S. C. Zimmerman, unpublished work.

Paper 7/00581D; *Received* 24*th January*, 1997